Systemic PaO2 oscillations cause mild brain injury in a pig model

Klein, Klaus U ; Johannes, Amelie ; Brückner, Melanie ; Thomas, Rainer ; Matthews, Stephan ; Frauenknecht, Katrin ; Leukel, Petra ; Mazur, Johanna ; Poplawski, Alicia ; Muellenbach, Ralf ; Sommer, Clemens J ; Thal, Serge C ; Engelhard, Kristin

Abstract: OBJECTIVE: Systemic PaO2 oscillations occur during cyclic recruitment and derecruitment of atelectasis in acute respiratory failure and might harm brain tissue integrity. DESIGN: Controlled animal study. SETTING: University research laboratory. SUBJECTS: Adult anesthetized pigs. INTERVENTIONS: Pigs were randomized to a control group (anesthesia and extracorporeal circulation for 20 hr with constant PaO2, n = 10) or an oscillation group (anesthesia and extracorporeal circulation for 20 hr with artificial PaO2 oscillations [3 cycles min ^{1}], n = 10). Five additional animals served as native group (n = 5). MEASUREMENTS AND MAIN RESULTS: Outcome following exposure to artificial PaO2 oscillations compared with constant PaO2 levels was measured using 1) immunohistochemistry, 2) real-time polymerase chain reaction for inflammatory markers, 3) receptor autoradiography, and 4) transcriptome analysis in the hippocampus. Our study shows that PaO2 oscillations are transmitted to brain tissue as detected by novel ultrarapid oxygen sensing technology. PaO2 oscillations cause significant decrease in NISSL-stained neurons ($p < 0.05$) and induce inflammation ($p < 0.05$) in the hippocampus and a shift of the balance of hippocampal neurotransmitter receptor densities toward inhibition ($p < 0.05$). A pathway analysis suggests that cerebral immune and acute-phase response may play a role in mediating PaO2 oscillation-induced brain injury. CONCLUSIONS: Artificial PaO2 oscillations cause mild brain injury mediated by inflammatory pathways. Although artificial PaO2 oscillations and endogenous PaO2 oscillations in lung-diseased patients have different origins, it is likely that they share the same noxious effect on the brain. Therefore, PaO2 oscillations might represent a newly detected pathway potentially contributing to the crosstalk between acute lung and remote brain injury.

DOI: https://doi.org/10.1097/CCM.0000000000001399

Systemic Pao_2 Oscillations Cause Mild Brain Injury in a Pig Model

Klaus U. Klein, MD[1,2]; Amelie Johannes, MD[2,3]; Melanie Brückner, DVM[1]; Rainer Thomas, MD[1]; Stephan Matthews, MD[1]; Katrin Frauenknecht, MD[4]; Petra Leukel, PhD[4]; Johanna Mazur, PhD[5]; Alicia Poplawski, PhD[6]; Ralf Muellenbach, MD[3]; Clemens J. Sommer, MD[4]; Serge C. Thal, MD[1]; Kristin Engelhard, MD[1]

Objective: Systemic Pao_2 oscillations occur during cyclic recruitment and derecruitment of atelectasis in acute respiratory failure and might harm brain tissue integrity.

Design: Controlled animal study.

Setting: University research laboratory.

Subjects: Adult anesthetized pigs.

Interventions: Pigs were randomized to a control group (anesthesia and extracorporeal circulation for 20 hr with constant Pao_2, $n = 10$) or an oscillation group (anesthesia and extracorporeal circulation for 20 hr with artificial Pao_2 oscillations [3 cycles min^{-1}], $n = 10$). Five additional animals served as native group ($n = 5$).

Measurements and Main Results: Outcome following exposure to artificial Pao_2 oscillations compared with constant Pao_2 levels was measured using 1) immunohistochemistry, 2) real-time polymerase chain reaction for inflammatory markers, 3) receptor autoradiography, and 4) transcriptome analysis in the hippocampus. Our study shows that Pao_2 oscillations are transmitted to brain tissue as detected by novel ultrarapid oxygen sensing technology. Pao_2 oscillations cause significant decrease in NISSL-stained neurons ($p < 0.05$) and induce inflammation ($p < 0.05$) in the hippocampus and a shift of the balance of hippocampal neurotransmitter receptor densities toward inhibition ($p < 0.05$). A pathway analysis suggests that cerebral immune and acute-phase response may play a role in mediating Pao_2 oscillation–induced brain injury.

Conclusions: Artificial Pao_2 oscillations cause mild brain injury mediated by inflammatory pathways. Although artificial Pao_2 oscillations and endogenous Pao_2 oscillations in lung-diseased patients have different origins, it is likely that they share the same noxious effect on the brain. Therefore, Pao_2 oscillations might represent a newly detected pathway potentially contributing to the crosstalk between acute lung and remote brain injury. (*Crit Care Med* 2016; 44:e253–e263)

Key Words: acute brain injury; acute lung injury; acute respiratory distress syndrome; cyclic recruitment of atelectasis; neuroinflammation; oxygen oscillations

[1]Department of Anaesthesiology, University Medical Center of the Johannes Gutenberg-University, Mainz, Germany.

[2]Department of Anaesthesia, General Intensive Care and Pain Management, Medical University of Vienna, Vienna, Austria.

[3]Department of Anaesthesia and Critical Care, University Hospitals, Wuerzburg, Germany.

[4]Institute of Neuropathology, University Medical Center of the Johannes Gutenberg-University, Mainz, Germany.

[5]Core Facility Bioinformatics, Division Biostatistics and Bioinformatics, Institute of Medical Biostatistics, Epidemiology and Informatics, University Medical Center of the Johannes Gutenberg-University, Mainz, Germany.

[6]Division Biostatistics and Bioinformatics, Institute of Medical Biostatistics, Epidemiology and Informatics, University Medical Center of the Johannes Gutenberg-University, Mainz, Germany.

Data presented in this article are part of a doctoral thesis presented by Stephan Matthews to the Medical Faculty of the Johannes Gutenberg-University, Mainz, Germany, and a doctoral thesis presented by Annett Geissendörfer to the Medical Faculty of the Julius-Maximilian-University of Würzburg, Germany.

Supplemental digital content is available for this article. Direct URL citations appear in the printed text and are provided in the HTML and PDF versions of this article on the journal´s website (http://journals.lww.com/ccmjournal).

Supported by a research grant of the German Research Foundation (DFG Pak 415, EN 904/1-1).

Dr. Engelhard received funding from the German Research Foundation and funding from AbbVie and Fresenius Kabi. Dr. Thal received funding from the German Research Foundation and from the German Federal Ministry of Research and Education. Dr. Sommer received funding from the German Research Foundation, provided expert testimony for the Public attorney´s office, and and has a patent with Syngis GmbH. The remaining authors have disclosed that they do not have any potential conflicts of interest.

For information regarding this article, E-mail: ulrich.klein@meduniwien.ac.at

DOI: 10.1097/CCM.0000000000001399

Despite improvements in critical care medicine, mortality rate of patients with severe acute respiratory distress syndrome (ARDS) still hovers around 30–40% (1). However, most patients do not die of acute respiratory failure (1st hit)—but rather from secondary multiple organ failure (2nd hit). The classical conception of this secondary multiple organ injury following ARDS proposes that biotrauma causes systemic inflammation resulting in remote organ injury (2).

Although systemic inflammation is certainly one major contributor to remote organ injury after ARDS, it seems unlikely to be the solitary pathomechanism.

A novel concept postulates that oxygen oscillations caused by cyclic recruitment and derecruitment of atelectasis (cyclic R/D) during ARDS may contribute to secondary organ injury (3). Within-breath cyclic R/D results in varying shunt fraction and altered gas exchange, thereby causing high-amplitude respiratory-dependent Pa_{O_2} oscillations (Pa_{O_2} oscillations) (4, 5). These Pa_{O_2} oscillations travel with the systemic circulation to remote organs (6, 7). However, the impact of Pa_{O_2} oscillations on remote organs such as the brain has not yet been investigated.

Previous animal experiments showed that high-amplitude Pa_{O_2} oscillations occur during experimental ARDS (4–8). The amplitude of these endogenous Pa_{O_2} oscillations may differ largely between subjects making in vivo intergroup comparisons challenging. Therefore, as a novel approach, we used an extracorporeal membrane oxygenation (ECMO) circulatory model that fully replaces normal circulation using nonpulsatile constant blood flow to investigate the effects of artificially generated Pa_{O_2} oscillations on brain tissue integrity. We hypothesized that artificial Pa_{O_2} oscillations applied for 20 hours would cause brain injury as quantified by immunohistochemistry, inflammatory marker gene expression, and receptor autoradiography in the hippocampus. A pathway analysis based on genomic profiling was performed to potentially unravel underlying pathomechanisms.

MATERIALS AND METHODS

This study was approved by the State and Institutional Animal Care Committee (Regierung von Unterfranken, Würzburg, Germany, 55.2-2531.01-89/10). Five pilot experiments (Pietrien race, weight 50–60 kg) were conducted to develop the experimental setup and feasibility of the protocol. Five pigs were investigated as native pigs (anesthesia for 30 min, $n = 5$). Thereafter, 20 adult pigs (Pietrien race, weight 50–60 kg) were investigated in a randomized study (control group, $n = 10$ animals; oscillation group, $n = 10$ animals). For a detailed description of the preparation of the pigs, including the ECMO for the generation of artificial Pa_{O_2} oscillations and the craniotomy for the placement of an oxygen-sensing probe to verify that Pa_{O_2} oscillations are transmitted to the brain; see **Supplement 1** (Supplemental Digital Content 1, http://links.lww.com/CCM/B464).

After start of the ECMO, oscillating Pa_{O_2} in the intervention group was produced using a custom made computed controlled gas switch consisting of two mass flowmeters that allowed for purging between pure oxygen and pure nitrogen administered to the oxygenator of the ECMO device (EL-Flow select series; Bronkhorst, Ruurlo, The Netherlands). This novel model allowed for continuous nonpulsatile blood flow but constant (control group) or absolutely reproducible cyclically altered Pa_{O_2} levels (oscillation group, 3 cycles min^{-1}) to produce large artificial Pa_{O_2} oscillations with a target amplitude more than 150 torr (20 kPa). In the control group, the gas flow was set to maintain Pa_{O_2} constant within the range of 80–120 torr (10–16 kPa).

Experimental Protocol

After measurement of baseline values, ventricular fibrillation was induced by administration of 40 mmol potassium chloride and the ECMO was started at 2–3 L min^{-1} cardiac index (Marquet Rotaflow; Maquet, Rastatt, Germany). Animals were randomized into the following two groups: control group ($n = 10$), settings: anesthesia, intubation, instrumentation, and ECMO for 20 hours; Pa_{O_2} constant between 80 and 120 torr (10–16 kPa), Pa_{CO_2} 35–45 torr (4.6–5.9 kPa), tidal volume (V_T) 3 ml kg^{-1}, positive end-expiratory pressure (PEEP) 10 mbar, respiration rate (RR) 10–25 min^{-1}; oscillation group ($n = 10$), settings: anesthesia, intubation, instrumentation, and ECMO for 20 hours; Pa_{O_2} oscillating between 60 and more than 250 torr (8 to > 33 kPa), Pa_{CO_2} 35–45 torr (4.6–5.9 kPa), V_T 3 ml kg^{-1}, PEEP 10 mbar, RR 10–25 min^{-1}. At the end of the experiment, brains were removed and the hemispheres were separated. The right hemisphere was stored in formalin 4% (histologic analysis of hippocampus) and the left hemisphere was stored in soluble nitrogen at –80°C for molecular analysis and receptor-autoradiography of the hippocampus.

Ultrafast Pa_{O_2} Measurement

The ultrafast partial pressure of oxygen measurement (Foxy AL-300; Ocean Optics, Dunedin, FL) was used to continuously monitor Pa_{O_2} (torr) in the systemic circulation during experiments using an uncoated 10-Hz fluorescence quenching probe that was advanced via the left carotid artery into the thoracic aorta. This ultrathin probe allows a fibreoptic, aluminum-jacketed probe with an uncoated ruthenium complex at the probe tip. Before start of the experiments, accurate calibration of the probe was confirmed by conventional blood gas analysis (Rapidlab 248; Bayer Healthcare, Leverkusen, Germany).

Ultrafast Cerebral Hemoglobin Oxygen Saturation and Blood Flow Measurement

The oxygen-to-see (O_2C) technology was used for ultrafast measurement of cerebral hemoglobin oxygen saturation and blood flow to monitor cerebral capillary venous oxygen hemoglobin saturation (So_2), cerebral capillary venous blood flow (CBF), and cerebral capillary venous blood flow velocity (CBFV) simultaneously in 2- and 8-mm cerebral depth (O_2C-device; Lea Medizintechnik GmbH, Giessen, Germany) (9–11). This technology was used to confirm that during the experiment, Pa_{O_2} oscillations were transmitted with the systemic circulation to the brain. Parameters were measured by combined 2.5-Hz white light spectroscopy and 20-Hz laser Doppler flowmetry. The underlying principle is based on detection of multiple white light wavelength (500–600 nm, < 30 mW) and comparison to universal reference values of deoxygenated and oxygenated hemoglobin spectra to determine So_2. Illuminated laser light (830 nm, < 30 mW) is used to calculate a Doppler shift caused by movements of erythrocytes and used for analysis of CBF and CBFV. The probe was applied onto the intact

dura for simultaneous measurements of all parameters at the capillary-venous level of cerebral microcirculation.

Histologic Analysis of Neuronal Injury

Hippocampus brain region was trimmed and cut into 50-μm vibratome sections. Samples were preserved in phosphate-buffered saline with sodium azide. For quantification of neuronal cell count, four levels (0, 150, 300, and 450 μm) were selected at 150-μm interval. After mounting on gelatin-coated slides and air drying, sections were stained with cresyl violet according to NISSL. At each level, cornu ammonis (CA) 1, CA2, and CA4 regions of the hippocampus were evaluated for the number of viable neurons (CA1, CA2: number of neurons/0.1×0.28 mm area; CA4: number of neurons/0.2×0.28 mm) to determine the mean neuronal density with a Zeiss Axiovert microscope and Zeiss AxioVision Microscope Software (Zeiss, Oberkochen, Germany) at 40× magnification. Cells that were located completely inside the frame and cells that crossed only through its top or right side were counted. Cells crossing the planes that define the bottom and left side of the frame were not counted (12). Viable (counted) cells fulfilled the following criteria: sharply delineated nucleus, clearly distinguishable nucleolus located centrally within the nucleus, neuronal cytoplasm clearly demarcated from surrounding neuropil, and less than one third of the neuron surrounded by confluent vacuolization (13). To avoid accidental counting of nonneuronal apoptotic/pyknotic cells (e.g., endothelial and glial cells), apoptotic and pyknotic cells were excluded from analysis. Using NISSL-stained sections, classic ischemic neuron pathology with eosinophilic cytoplasm was not analyzed. An investigator blinded to the group allocation of the investigated animals determined histologic damage.

α-Amino-3-Hydroxy-5-Methyl-4-Isoxazolepropionic Acid Receptor and Gamma-aminobutyric Acid$_A$ Receptor Ligand-Binding Density

The frozen tissue was serially cut at –20°C into 20-μm-thick cryostat sections, and slices were mounted on triethoxysilylpropylamine-coated slides. To analyze binding densities of the excitatory α-amino-3-hydroxy-5-methyl-4-isoxazolepropionic acid receptor (AMPA) receptor and the inhibitory gamma-aminobutyric acid $(GABA)_A$ receptor, the brain slices were incubated with the respective tritium-labeled ligand, as described before (14, 15). Ligands were purchased from Perkin Elmer (Boston, MA). Labeling of and incubation procedures for the AMPA and $GABA_A$ binding sites were performed according to the protocols by Zilles et al (16, 17). Autoradiographies were scanned under equal lighting conditions using the digital CoolSNAP camera (Photometrics CoolSNAP; Roper Scientific, Ottobrunn, Munich, Germany) and were then digitized with an image analysis system (Imaging Research, St. Catharines, ON, Canada). A nonlinear calibration curve, defining a relationship between gray values in the autoradiographs and concentrations of radioactivity, was generated using gray value images of the coexposed plastic standards. Semiquantitative analysis of ligand binding was performed in several hippocampal regions of interest including the pyramidal layer and dendritic layers of the CA1 and CA3 as well as the granular layer and molecular layer of the dentate gyrus (DG).

Analysis of Markers of Inflammation

Frozen brain tissues were analyzed for inflammatory cytokines (interleukin [IL]-1β, IL-6, and tumor necrosis factor [TNF]-α) as determined by real-time polymerase chain reaction (PCR) as described in detail previously (18). Plasma levels of inflammatory cytokines (IL-1β, IL-6, and TNF-α) were determined at baseline and at 8, 16, and 20 hours by means of enzyme-linked immunosorbent assays (Porcine Quantikine ELISA Kit; R&D Systems, Minneapolis, MN).

Transcriptome and Pathway Analysis

Transcriptome and pathway analysis from hippocampal tissue was performed in two animals of the control group and two animals of the Pao_2 oscillations group. Complementary RNA (cRNA) synthesis and gene expression profiling: total RNA was isolated with the RNeasy mini kit (Qiagen, Valencia, CA) according to the manufacturer's instructions. Preparation of cRNA, hybridization to GeneChip Porcine Genome Array (Affymetrix, Santa Clara, CA), and scanning of the arrays were carried out as described according to the manufacturer's protocols (https://www.affymetrix.com). Images were analyzed with GeneChip software (Affymetrix, version 5.0). Scanner images were preprocessed using Affymetrix Gene Chip Operating Software.

Statistical Analysis

All data are presented as mean ± SD. A p value of less than 0.05 was considered statistically significant. Spirometric, hemodynamic, blood gas analysis, Pao_2 (Foxy AL-300), O_2C (So_2, CBF, CBFV), real-time PCR (IL-1β, IL-6, TNF-α) of brain tissue, serum cytokine levels (IL-1β, IL-6, TNF-α), and histologic data between the control group and the oscillation group were performed for each time point using the Mann-Whitney U test. Analyses were performed using Prism 6 (GraphPad Software, La Jolla, CA). Significant group effects for AMPA and $GABA_A$ receptor ligand-binding density were confirmed by one-way analysis of variance and Bonferroni error protection. Analysis was performed using the general statistics module of Analyse-it for Microsoft Excel (Analyse-it Software, Leeds, United Kingdom). Values are mean ± SD presented as percentage of ligand binding of sham brains. O_2C data frequency domain and waveform analysis were performed using Mathcad (Mathcard 2000; Mathsoft, Cambridge, MA) and Igor Pro (Igor Pro 6.22a; WaveMetrics, Lake Oswego, OR). For the analysis of microarray data, empirical Bayes method was applied by using the statistical software R (v 3.1.1) with the limma package (v 3.20.9) (19, 20). Pathway analysis was performed by using the software Ingenuity Pathway Analysis with the human genome database as reference.

RESULTS

The following animals died during the experiments and were excluded from the study: control group: two animals (causes: one ventricular fibrillation after guide-wire placement during

preparation; one pericardial tamponade after dilatator placement during preparation); oscillation group: three animals (causes: two death for unknown reasons during preparation; one severe lung hemorrhage after 10 hr). Consequently, eight animals of the control group, seven animals of the oscillation group, and five animals of the native group were included in the final analysis.

Hemodynamic and Spirometric Measurements

The applied respiratory parameters, hemodynamic variables, and results of the blood gas analysis during the experiments are summarized (Tables 1 and 2). No differences between groups could be observed with the exception that the oscillation group showed an increase in lactate levels after 16 hours (Table 2) ($p < 0.05$).

Systemic and Cerebral Pao_2/So_2/CBF/CBFV Oscillations

In the thoracic aorta, Pao_2 (Foxy AL-300) of the control group remained within a normal range (Pao_2 103 ± 18 torr [13.7 ± 2.4 kPa]; exemplary **Fig. 1*A***). Pao_2 in the oscillation group showed high-amplitude oscillations (mean Pao_2 amplitude, 340 ± 122 torr [45.3–16.3 kPa]; exemplary **Fig. 1*B***) as summarized in **Table 3**. In the control group, spontaneous oscillations in CBF and CBFV (O_2C) occurred in a low-frequency range (0.036–0.4 Hz) (Fig. 1*A* and Table 3). In the oscillation group, cyclically altered Pao_2 values were transmitted to the brain as confirmed by So_2, CBF, and CBFV (3 cycles min^{-1} = 0.05 Hz) (Fig. 1*B* and **Table 4**). In two animals of the control group and in five animals of the oscillation group, O_2C variables were measured accurately. In other animals, O_2C variables could not be measured accurately because small amounts of blood in the craniotomy field interfered with the signal during supine position.

Histologic Damage of Neuronal Tissue

In the CA1 and CA2 regions, less viable NISSL-stained neurons were detected in the oscillation group compared with the control group ($p < 0.05$) (**Fig. 2, *C* and *D***). A similar trend was observed in the CA4 region; however, no statistical significance could be reached (**Fig. 2*E***).

Markers of Inflammation

The messenger RNA expression of cerebral IL-1β was higher in the oscillation group compared with control group ($p < 0.05$) (**Fig. 3*A***). There was a trend for elevated TNF-α expression in the Pao_2 oscillation group compared with the control group (**Fig. 3*B***). For IL-6 expression, no significant difference was detected between groups (**Fig. 3*C***). Blood plasma levels of inflammatory markers (Il-1β, IL-6, and TNF-α) did not significantly differ between groups (**Supplemental** Fig. 1 A–C, Supplemental Digital Content 2, http://links.lww.com/CCM/B465).

TABLE 1. Spirometric and Hemodynamic Variables During Experiments

	Fio_2 (%)		Positive End-Expiratory Pressure (mbar)		Mean Airway Pressure (mbar)		Respiration Rate (min^{-1})		Tidal Volume (mL)		Minute Volume (L min^{-1})	
Timepoint	Control	Oscillation	Control	Oscillation	Control	Oscillation	Control	Oscillation	Control	Oscillation	Control	Oscillation
Baseline	0.3±0.1	0.3±0.1	5±1	5.6±2	8.3±0.8	9.1±1.8	21.4±4	23.4±5.9	236±29	225±23	4.7±0.6	5.0±1.4
ECMO	0.3±0.1	0.3±0.1	10.2±0.8	10.3±0.5	11.7±1.2	11.6±1.0	10.3±2.4	12.3±6.4	110±11	109±11	0.8±0.3	1.4±1.5
4 hr	0.4±0.1	0.3±0.1	10.3±0.5	10.6±0.5	11.5±0.8	12.0±0	11.5±2.3	8.7±2.2	111±14	110±15	0.8±0.4	0.7±0.3
8 hr	0.3±0.0	0.3±0.1	9.7±0.5	10.6±0.5	11.2±0.8	11.9±0.4	12.7±3.3	9.1±3.1	108±11	102±16	1.0±0.5	0.7±0.4
12 hr	0.3±0.0	0.3±0.1	9.9±0.4	10.3±0.8	11.1±0.7	12.7±1.8	15.0±2.9	11.3±3.4	109±17	105±11	1.2±0.7	1.1±0.7
16 hr	0.3±0.0	0.3±0.1	11.1±2.7	10±0	13.1±3.7	13.7±4.5	14.9±3.7	13.0±4.5	110±14	108±10	1.2±0.6	1.1±0.6
20 hr	0.3±0.0	0.3±0.1	11.0±2.8	10.2±0.4	13.6±4.1	13.8±5.3	16.1±4.8	13.8±5.3	110±11	107±11	1.3±0.6	1.3±0.7

	Heart Rate (min^{-1})		Mean Arterial Pressure (mm Hg)		Cardiac Index (L min^{-1})		Sweep o_2 (L min^{-1})		Pericranial Temperature (°C)		Spo_2 (%)	
Timepoint	Control	Oscillation	Control	Oscillation	Control	Oscillation	Control	Oscillation	Control	Oscillation	Control	Oscillation
Baseline	66±11	56±15	94.6±10.8	93.4±7.8	NA	NA	NA	NA	32.3±0.6	33.9±0.9	96±6	99±1
ECMO	151±39	141±38	76.5±17.3	79.7±13.6	2.4±0.2	2.0±0.5	2.0±0.1	2.0±0.2	33.4±2.0	34.8±1.3	100±0	94±8
4 hr	172±36	188±32	89.2±10.8	84.6±12.9	2.2±0.4	2.1±0.3	1.6±0.5	2.1±0.3	37.5±0.3	37.5±0.4	96±0.7	99±1
8 hr	153±30	177±6	77.8±11.8	84.6±11.5	2.4±0.2	2.1±0.1	2.0±0.3	2.2±0.3	37.4±0.3	37.6±0.4	NM	84±4
12 hr	163±34	193±30	74.7±7.7	74.7±7.3	2.6±0.5	2.1±0.2	2.3±1.1	2.2±0.4	37.5±0.5	37.4±0.5	NM	NM
16 hr	146±26	177±36	70.4±4.2	73.9±6.8	2.5±0.5	2.3±0.3	2.5±1.1	2.2±0.2	37.4±0.3	37.4±0.5	NM	NM
20 hr	170±16	184±23	71.7±3.3	77.6±9.1	2.5±0.5	2.3±0.2	3.0±1.1	2.3±0.2	37.2±0.4	37.6±0.3	NM	NM

ECMO = extracorporeal membrane oxygenation, Sweep = sweep gas flow, Spo_2 = peripheral hemoglobin oxygen saturation, NA = not applicable, NM = not measurable.

[a]$p < 0.05$ (control group vs. Pao_2 oscillation group).

Data are presented as mean (SD). Comparisons between control and Pao_2 oscillation group were performed using the Mann-Whitney *U* test.

TABLE 2. Blood Gas Analysis Variables During Experiments

Timepoint	pH		Pao_2 (torr)		$Paco_2$ (torr)		Hemoglobin (mg/dL)		Lactate (mmol/L)		Glucose (mg/dL)	
	Control	Oscillation	Control	Oscillation	Control	Oscillation	Control	Oscillation	Control	Oscillation	Control	Oscillation
Baseline	7.46±0.1	7.42±0.1	150±51	132±25	46.4±5.9	51.0±12.6	9.5±1.3	9.7±1.5	2.1±1.6	1.6±1.0	89±17	71±14
Extracorporeal membrane oxygenation	7.6±0.1	7.57±0.1	402±224	418±187	33.5±4.7	34.3±7.0	7.3±0.9	9.0±1.4	2.7±0.5	2.7±1.6	107±19	107±21
4 hr	7.47±0.1	7.52±0.1	101±27	156±133	45.6±8.6	39.5±6.9	8.7±1.2	9.1±1.6	1.3±0.2	2.6±2.0	127±55	106±32
8 hr	7.44±0.1	7.46±0.1	118±33	115±104	47.2±8.9	42.0±5.3	8.6±2.6	9.1±1.7	2.6±1.4	2.6±2.5	133±28	105±26
12 hr	7.47±0.0	7.46±0.1	115±20	176±114	44.1±6.1	45.6±4.8	8.2±1.8	8.3±2.2	1.7±1.4	2.8±2.1	117±36	109±25
16 hr	7.45±0.0	7.42±0.1	112±19	169±85	47.9±6.9	46.6±5.2	7.3±1.3	7.7±1.3	1.3±0.7	5.1±6.3[a]	110±34	117±34
20 hr	7.47±0.1	7.43±0.1	123±20	201±79	49.4±7.0	44.3±7.8	7.5±0.8	7.3±0.7	2.5±1.8	6.2±6.9[a]	86±19	132±61

[a]$p < 0.05$.

Pao_2 oscillation group showed an increase in lactate levels at the end of the experiment ($p < 0.05$). Data are presented as mean (SD). Comparisons between control and Pao_2 oscillation group were performed using the Mann-Whitney *U* test.

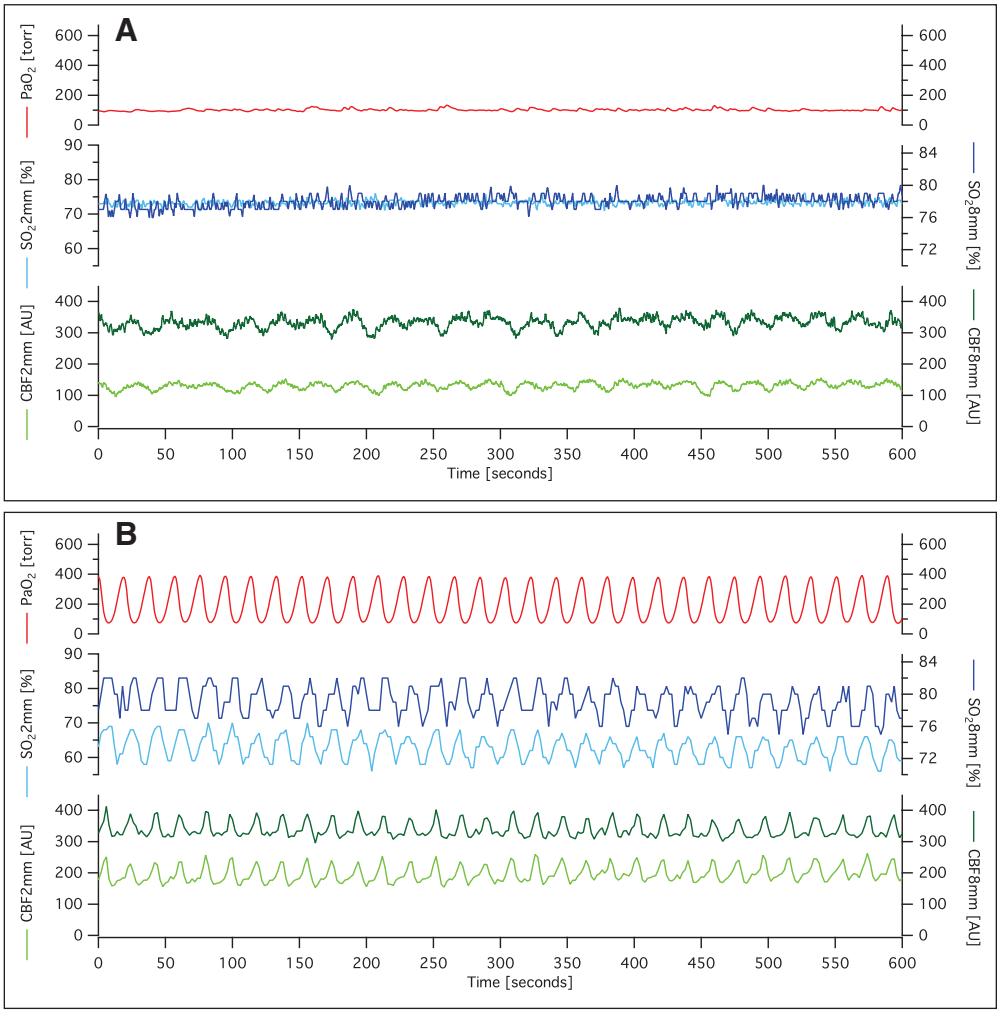

Figure 1. A, Control group animals showed that thoracic Pao_2 and cerebral capillary venous hemoglobin oxygen saturation (So_2) remained stable, while cerebral blood flow (CBF) and CBF velocity in 2- and 8-mm cerebral depth showed spontaneous CBF oscillations in the low-frequency range (0.036–0.4 Hz) during extracorporeal membrane oxygenation (ECMO) laminar flow. **B**, Pao_2 oscillation group animals showed that Pao_2 oscillations were transmitted to the brain and induced So_2 and CBF oscillations in 2 and 8 mm depth in the frequency set (0.05 Hz, 3 cycles min^{-1}) during ECMO laminar flow.

AMPA and $GABA_A$ Receptor Ligand-Binding Density

[^{3}H]AMPA ligand-binding density was decreased in the oscillation group compared with the control group in hippocampal (**Fig. 4*A***) CA1 and DG regions ($p < 0.05$) and trendwise in the CA3 region (**Fig. 4*B***). $GABA_A$ receptor autoradiography showed an increased ligand-binding density of [^{3}H]Muscimol in the DG of the oscillation group compared with the control group ($p < 0.05$) and trendwise the CA-1 and CA-3 regions (**Fig. 4*C***).

Transcriptome and Pathway Analysis

Transcriptome profiling by pathway analysis of hippocampal tissue revealed that 19 pathways ($p < 0.01$) play a role in O_2-oscillations-mediated cerebral injury with key regulation on inflammation and acute-phase response (**Fig. 5**).

DISCUSSION

The present study demonstrates that artificial Pao_2 oscillations applied for 20 hours induce mild

TABLE 3. Pao_2 of the Control Group and Oscillation Group

Experiment (no.)	Pao_2 Constant (torr)		Pao_2 Oscillation Amplitude (torr)		Pao_2 Oscillation Amplitude Minimum Value (torr)		Pao_2 Oscillation Amplitude Maximum Value (torr)	
	Control	Oscillation	Control	Oscillation	Control	Oscillation	Control	Oscillation
1	103±12	NA	NA	238±89	NA	67±11	NA	304±95
2	102±7	NA	NA	286±95	NA	76±25	NA	362±98
3	94±12	NA	NA	377±88	NA	72±13	NA	449±96
4	107±3	NA	NA	325±99	NA	81±10	NA	406±95
5	85±15	NA	NA	455±109	NA	76±15	NA	531±114
6	107±15	NA	NA	246±71	NA	70±8	NA	316±71
7	116±33	NA	NA	451±69	NA	68±9	NA	518±74
Mean ± SD	103±18	NA	NA	340±122	NA	73±15	NA	412±124

NA = not applicable.

[a]$p < 0.05$.

Results demonstrate that the control group showed a constant Pao_2 (103±18 torr), whereas the Pao_2 oscillation group showed a changing Pao_2 (amplitude 340±122 torr at a cycling frequency of 3 min^{-1}).

Data are presented as mean (SD). Comparisons between control and Pao_2 oscillation group were performed using the Mann-Whitney *U* test.

hippocampal injury, possibly mediated by cerebral inflammation. The up-regulation of the binding densities of the inhibitory $GABA_A$ receptors and the down-regulation of the binding densities to the excitatory AMPA receptors in the oscillation group resulting in a shift toward inhibition may represent an endogenous protective mechanism caused by stress to hippocampal cells (21). Pathway analysis suggests that numerous pathways may play a role in artificial Pao_2 oscillation–induced cerebral injury, including immune and acute-phase response. Possibly, also endogenous Pao_2 oscillations, which clinically occur during cyclic R/D in respiratory failure, may have a similar effect like the artificial Pao_2 oscillations and, thereby, represent a newly detected independent pathomechanism in the crosstalk between acute lung and brain injury.

Systemic and Peripheral Oxygen Oscillations

Early in 1911, Krogh and Lindhard proposed that Pao_2 might fluctuate during normal respiration (e.g., 10 torr). However, since 1966, respiratory-dependent variations of blood oxygenation (e.g., 5–439 torr) caused by varying shunt fraction were evidenced in small and large animal models (4, 5, 22, 23). These blood oxygen oscillations are translated into Pao_2 (and peripheral hemoglobin oxygenation saturation; Spo_2) oscillations and transmitted with the circulation to organs (6, 7). The impact of these oxygen oscillations on organ tissue (i.e., brain, heart, and kidney) integrity has not been investigated. While in all previous studies, Pao_2 (or Spo_2) oscillations were caused by cyclic R/D, high-amplitude Pao_2 oscillations in the present study were produced artificially (Fig. 1*B*). The

TABLE 4. Cerebral Microcirculation (O_2C Device) During Experiments

Timepoint	So_2_P1S (%)		So_2_P2D (%)		CBF_P1S (AU)		CBF_P2D (AU)		CBFV_P1S (AU)		CBFV_P2D (AU)	
	Control	Oscillation	Control	Oscillation	Control	Oscillation	Control	Oscillation	Control	Oscillation	Control	Oscillation
Baseline	70±12	79±13	77±2	79±7	192±49	210±87	255±50	252±24	25±4	31±7	33±4	37±6
Extracorporeal membrane oxygenation	62±15	61±22	74±13	76±3	327±225	204±85	445±14	271±39	40±23	30±8	46±1	38±2
4 hr	62±2	70±10	72±9	75±2	277±223	148±109	476±272	281±131	36±21	24±3	43±16	40±10
8 hr	51±25	61±23	78±1	82±8	175±88	220±120	336±35	248±80	23±4	29±6	34±3	34±1
12 hr	50±33	56±31	76±2	81±8	185±80	163±93	371±60	272±70	23±6	28±16	36±6	38±5
16 hr	83±0	62±41	79±0	76±7	94±0	146±36	200±0	282±142	16±0	27±12	22±0	35±8
20 hr	71±0	47±29	77±0	81±13	39±0	147±82	26±0	189±108	17±0	24±11	16±0	30±13

So_2 = cerebral capillary venous hemoglobin oxygen saturation, CBF = cerebral capillary venous blood flow, CBFV = cerebral capillary venous blood flow velocity, P1S = 2-mm depth, P2D = 8-mm depth.

[a]$p < 0.05$.

Cerebral capillary venous hemoglobin oxygen saturation, CBF, and CBFV in 2-mm depth (So_2_P1S, rHb_P1S, Flow_P1S, Velo_P1S) and in 8-mm cerebral depth (So_2_P2D, rHb_P2D, Flow_P2D, Velo_P2D). Data are presented as mean (SD). Comparisons between control and Pao_2 oscillation group were performed using the Mann-Whitney *U* test.

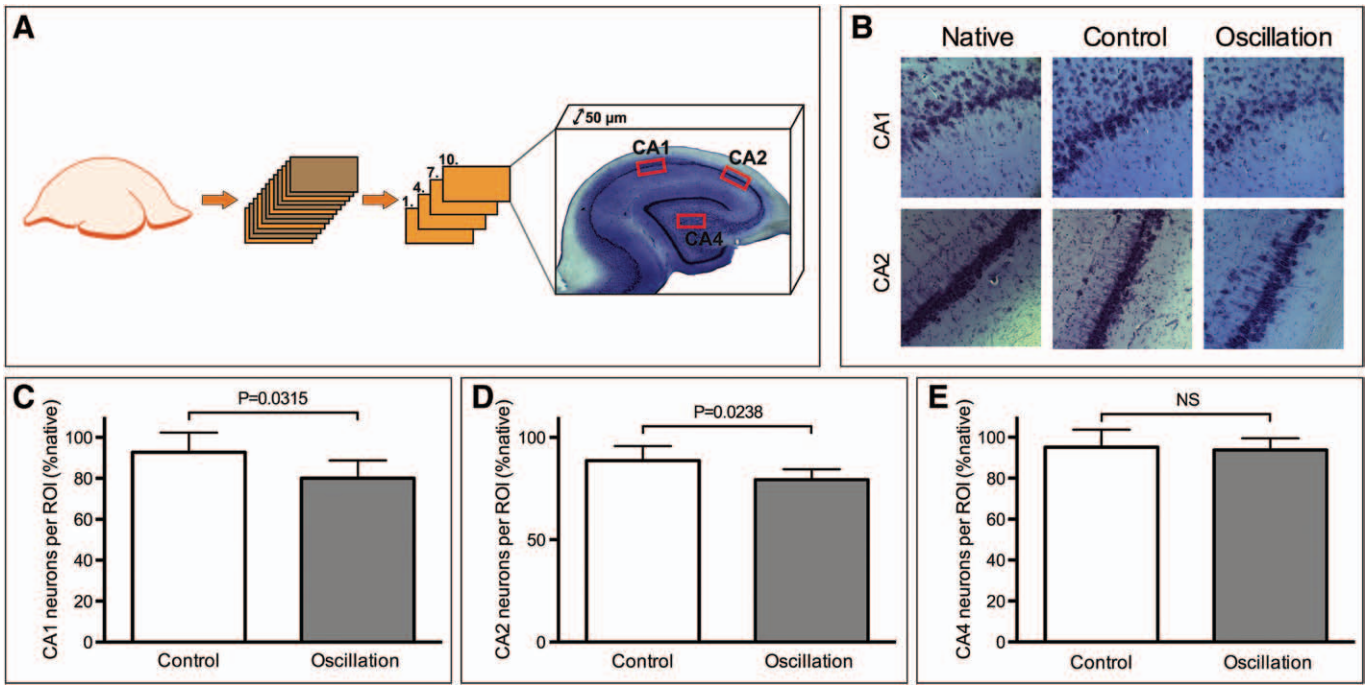

Figure 2. A, Regions of interest for the histopathologic analysis. **B**, NISSL staining in the CA-1 and CA-2 regions of the hippocampus. Pao_2 oscillation group showed more histopathologic damage (NISSL staining) in the CA1 region ($p = 0.0315$) (**C**) and CA2 region ($p = 0.0238$) (**D**) of the hippocampus compared with control group animals. **E**, No significant (NS) difference between groups was detected in the CA4 region. ROI = region of interest.

authors did choose this experimental approach since Pao_2 oscillations caused by cyclic R/D are variable in amplitude over time, and therefore, a standardized investigation of the potentially deleterious effect on the brain is difficult (6). Artificially produced Pao_2 oscillations remained stable during the whole study period. Any confounding impact from ARDS biotrauma can, therefore, be excluded in the present study.

Cerebral Oxygen Oscillations Cause Neuroinflammation

Artificial Pao_2 oscillations did cause a significant increase of cerebral inflammation (IL-1β) as compared with the control group. TNF-α as an alternative marker of cerebral inflammation showed a similar trend. This finding suggests that Pao_2 oscillations may be an independent cause for neuroinflammation. It is well known that a systemic inflammatory cascade is triggered by biotrauma in ARDS (24). Increased levels of inflammatory mediators (i.e., IL-1β, IL-6, and TNF-α) and circulating proapopotic soluble factors are responsible in this progress (25). However, additionally to this well-characterized pathomechanism, Pao_2 oscillations may enhance this inflammatory process and potentially worsen neurologic outcome after ARDS.

Pao_2 levels in our study did not range toward hypoxic levels. Instead, artificial Pao_2 oscillations in the present study did cause intermittent hyperoxia that also may occur in the presence of atelectrauma when Fio_2 is set to higher levels (6). It seems likely that Pao_2 oscillations would interfere with normal oxygen delivery to neuronal cells and finally to mitochondria, potentially disturbing mitochondrial oxygen homeostasis (26). As all enzymes in the human body and in each cell have an individual oxygen optimum, any fluctuation likely induces disturbances in the correct functioning of cellular enzymes (27). We observed an increase in lactate concentration in the Pao_2 oscillations group that potentially might be attributed to increased O_2-demand because of altered cellular Michaelis-Menten

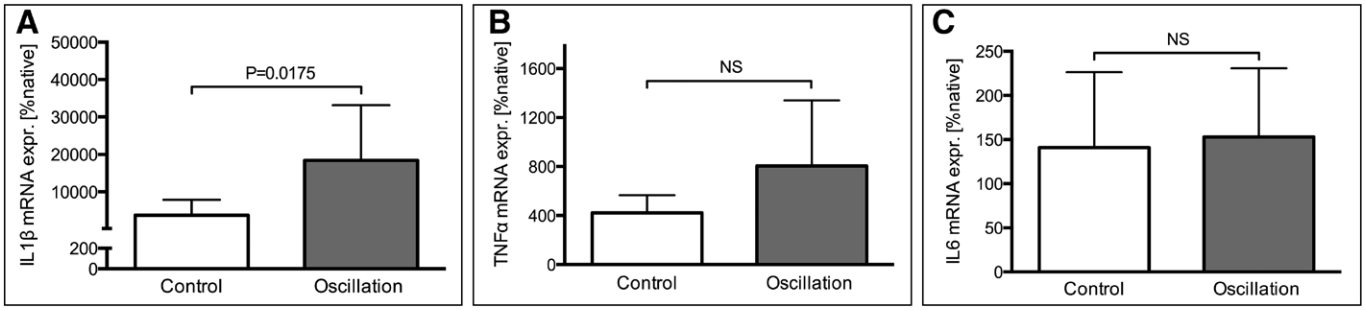

Figure 3. A, Pao_2 oscillation group showed more cerebral inflammation (interleukin [IL]-1β) in the hippocampus compared with control group animals ($p = 0.0175$). **B**, For tumor necrosis factor (TNF)-α expression, no significant (NS) difference was detected between groups. **C**, For IL-6 expression, NS difference was detected between groups. mRNA = messenger RNA.

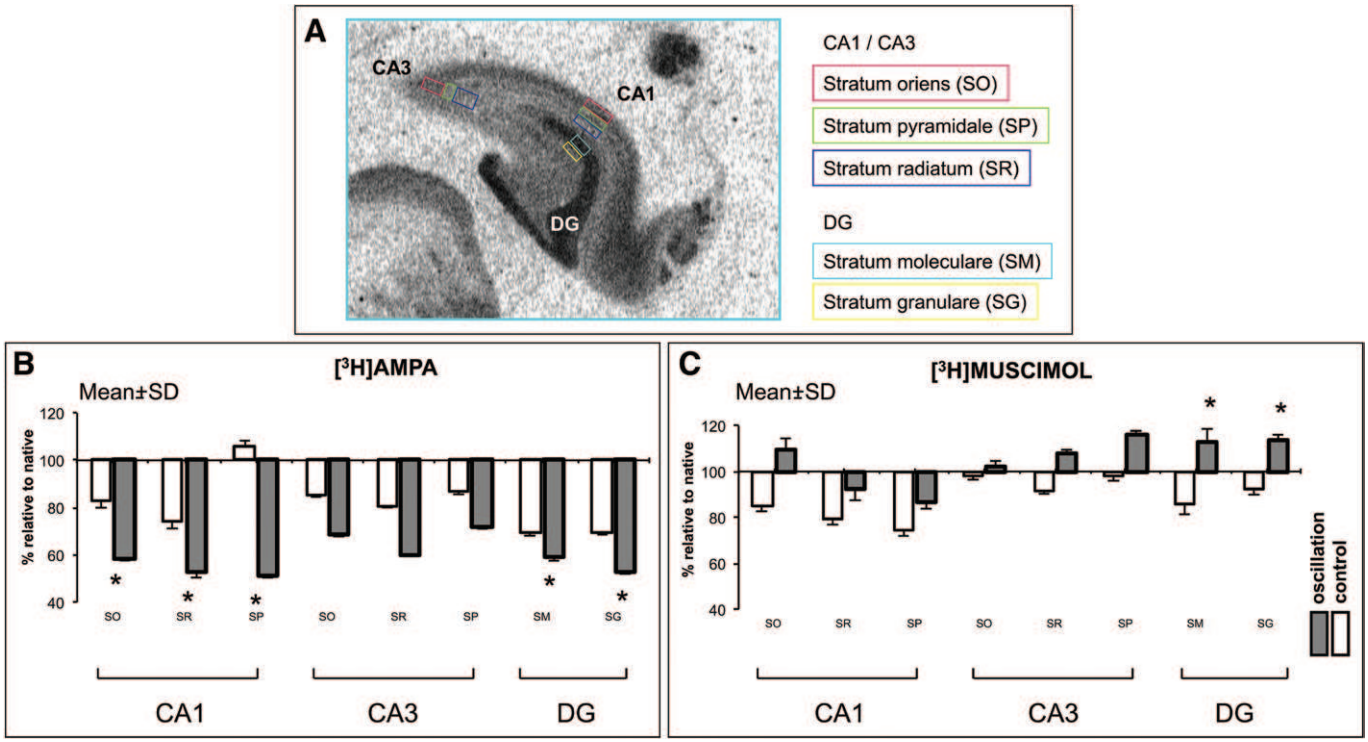

Figure 4. A, Regions of interest for analysis of neurotransmitter receptor binding densities. Representative autoradiography of a [^{3}H]Muscimol-incubated frozen brain section at the level of the hippocampus. Regions of interest are marked including the pyramidal layer and dendritic layers (stratum oriens and radiatum) of the CA1 and CA3 subregions as well as the granular and molecular layer of the dentate gyrus (DG). **B**, [^{3}H]AMPA ligand-binding density is significantly decreased in the oscillation group in the hippocampal regions CA1 and DG compared with the control group. **C**, $GABA_A$ receptor autoradiography showed an increased ligand-binding density of [^{3}H]Muscimol in the DG in the Pao_2 oscillation group compared with the control group.

kinetics. Pao_2 oscillations may also interfere with cell function by the production of reactive oxygen species. Furthermore, the present results demonstrate that control group showed an increase in inflammatory markers in comparison to the sham group that can be explained by the ECMO itself applied for a duration of 20 hours. It is well known that ECMO over a long period of time causes systemic and organ inflammation (28). Therefore, it is even more interesting that the effect of Pao_2 oscillations on cerebral inflammation was superimposed to the deleterious effect of ECMO therapy. Further, there was no difference between inflammatory (IL-1β, IL-6, and TNF-α) plasma levels; therefore, cerebral inflammation likely was not attributed to ECMO but rather to Pao_2 oscillations.

Cerebral Oxygen Oscillations Cause Neuronal Damage

Compared with the control group, Pao_2 oscillation group did result in increased brain damage in the CA1 and CA2 regions as measured by NISSL staining (Fig. 2). As the CA1 and 2 regions are most vulnerable to any ischemic or hypoxic challenge, an injury within this region is likely. As patients with ARDS are ventilated over days and weeks, a potential cerebral damage caused by Pao_2 oscillations may evolve over a long-time period. In the long term, Pao_2 oscillations theoretically could promote loss of brain tissue integrity and thereby cause neurocognitive impairments such as observed in patients with delirium (29). Although not investigated in the present study, it seems likely that reactive oxygen species- and reactive nitrogen species-associated mechanisms may be the underlying cause for brain damage after Pao_2 oscillations. Oxidative stress is caused both during intermittent hypoxia and hyperoxia, resulting in elevated toxic radical species formation, membrane lipid degradation through lipid peroxidation, protein oxidation, and oxidative DNA damage. In the brain, oxidative burden is even greater as neurons have only limited or no capacity for cell division or regeneration. Other respiratory diseases (i.e., asthma, chronic obstructive lung disease, and pulmonary fibrosis), as well as neurodegenerative diseases (i.e., Alzheimer, Parkinson, Huntington disease, and amyotrophic lateral sclerosis), have been linked to altered cellular oxygen levels (30–32). Likewise, although not measured, cerebral damage in the present study can be explained by impairment of redox homeostasis in the Pao_2 oscillation group on top of a systemic inflammation caused by ECMO therapy in the control group.

Cerebral Oxygen Oscillations Affect $GABA_A$/AMPA Receptors

The hippocampal $GABA_A$ ([^{3}H]Muscimol) receptor-binding densities are up-regulated in the Pao_2 oscillation group, reaching significance level in the DG region (Fig. 4). For the AMPA ([^{3}H]AMPA) receptor-binding densities, the results are contrariwise in all hippocampal regions (CA1 and DG) analyzed. These data imply that neuronal receptor binding densities may be altered in return to constant or oscillating Pao_2 levels. It has been demonstrated that severe neuronal injury (i.e., traumatic brain injury) leads to excessive release of glutamate and in return to

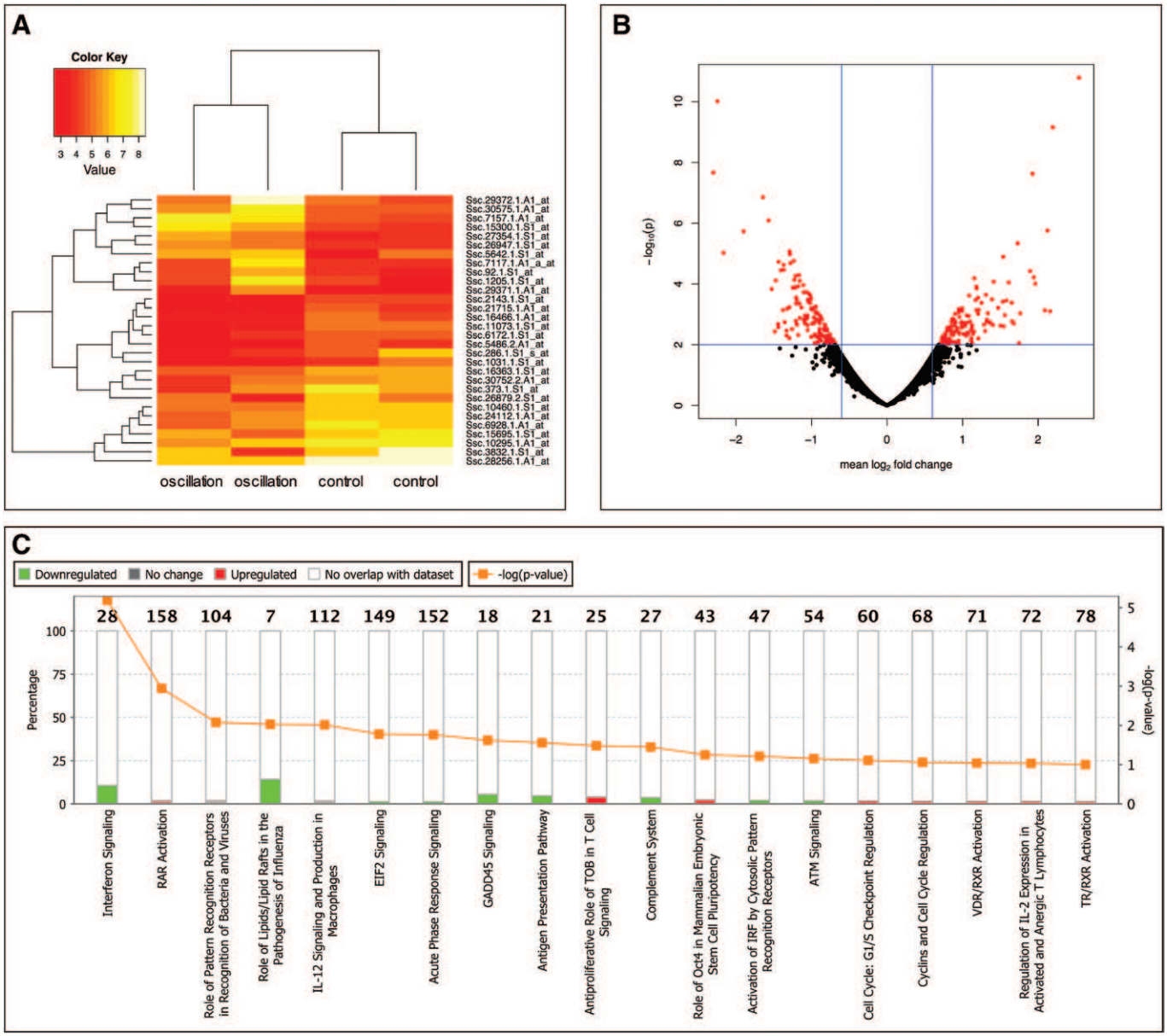

Figure 5. A, Heat map of microarray analysis for differential expression. The heat map shows the genes that are significantly (false discovery rate < 0.05) differentially expressed for Pao_2 oscillation group (*left*) versus control group (*right*). Bright color means strong gene expression. **B**, Volcano plot of microarray analysis for differential expression. *Red points* represent differentially expressed genes (p value < 0.01) with a $\log_2$-fold change more than 0.6 of hippocampal tissue of the oscillation groups versus the control group. **C**, Data show that a number of pathways are modulated during Pao_2 oscillations, including immune and acute-phase response.

down-regulation of excitatory neuronal receptors such as the *N*-methyl-D-aspartate receptor (33). Likewise, down-regulation of the binding densities of the [^{3}H]AMPA in the present study may hint toward neuronal injury in the Pao_2 oscillation group. At the same time, the increase of the binding densities for [^{3}H]Muscimol (inhibitory $GABA_A$ receptors) together with decreased ligand binding to AMPA receptors results in a shift to increased inhibition, which may indicate that protective pathways are stimulated during Pao_2 oscillations (21).

Cerebral Oxygen Oscillations Affect CBF

Artificial Pao_2 oscillations were transmitted to the brain and induced synchronized cerebral So_2 oscillations (Fig. 1). Such So_2 oscillations have been described before during cyclic recruitment and derecruitment of atelectasis during ARDS in pigs (6). In this former study, So_2 oscillations were accompanied by CBF oscillations (0.05 Hz, 3 cycles min^{-1}). This finding may be of paramount clinical importance, indicating that dynamic CBF regulation is not only dependent on changes in blood pressure but also largely depends on So_2. The present study confirms this observed phenomenon (6). Even during ECMO laminar flow, So_2 oscillations induced synchronized CBF oscillations and hint toward an extremely fast regulation of CBF and So_2. Such ultrarapid relationship has been described for CO_2 and CBF (34, 35), however, not for So_2 and CBF. Present cerebrovascular autoregulation models do not take into account this

ultrafast regulation of So_2 on CBF; therefore, the authors of the present study believe that this phenomenon is most relevant and needs further investigation.

Additionally to this finding, spontaneous CBF oscillations were observed in the control group (Fig. 1). While mean arterial pressure (MAP)-dependent CBF oscillations frequently are observed (36), spontaneous MAP independent CBF oscillations rarely have been described (37, 38). Interestingly, as the ECMO in the present study produced laminar MAP, spontaneous CBF oscillations at a frequency of 0.036–0.4 Hz must have been generated by the brain itself. It seems strange that the brain produces spontaneous CBF oscillations. However, similar infra-slow CBF oscillations (at a frequency of 0.06 Hz) have been described recently in patients undergoing nonpulsatile cardiopulmonary bypass (38). Although the purpose of spontaneous CBF oscillations remains unknown, it has been discussed that CBF oscillations promote cerebral vasomotion that largely (factor 8) might enhance oxygen diffusion to the brain (38–40). This conception would implicate that CBF oscillations might represent a physiologic protective mechanism that is activated in response to disturbed CBF for enhancement of cerebral oxygen delivery.

Limitations

The following methodological and technical limitations should be discussed. A main difference to a clinical ARDS scenario is that systemic circulation was produced by the ECMO. However, the authors decided to use the ECMO model because Pao_2 oscillations caused by atelectrauma cannot be easily reproduced steadily over a longer period of time. With the ECMO, it was possible to characterize the isolated effect of Pao_2 oscillations on neuronal integrity. We decided not to allow for spontaneous circulation as individual cardiac output and oxygenation largely blunt artificial Pao_2 oscillations generated by ECMO. This study design prevents from any circulatory adaptations in return to altered Pao_2 levels such as changes in cardiac output during Pao_2 extremes. Importantly, however, the results of the present study cannot be transferred to a clinical scenario as Pao_2 oscillations were induced artificially and not generated by cyclic R/D. Furthermore, artificial Pao_2 oscillations in the present study did range toward extreme hyperoxic values possibly inducing the generation of more free oxygen radicals. These high Pao_2 values cannot be expected during routine clinical ARDS therapy. However, endogenous Pao_2 oscillations potentially might show more deleterious effects on brain tissue integrity, as neuronal tissue might be preinjured by ARDS biotrauma. Another limitation is that porcine microarray data were analyzed using the human genome as a reference, potentially biasing results of the present study.

CONCLUSIONS

The present study reveals that artificial Pao_2 oscillations during extracorporeal circulation are forwarded to the brain, where they caused synchronized oxygen and blood flow oscillations. Artificial Pao_2 oscillations produce a mild brain injury as indicated by a reduced number of NISSL-stained neurons in the CA1 and CA2 region and an increase in cerebral inflammation (IL-1β). Pathway analysis supports this finding, indicating modulation of immune and acute-phase response by Pao_2 oscillations. In order to characterize the effect of Pao_2 oscillations on brain tissue without influencing factors, the Pao_2 oscillations were produced artificially in the present study and not caused endogenous by cyclic R/D during respiratory failure. The present study results suggest that artificial Pao_2 oscillations may cause direct cerebral injury, potentially representing a new pathway in the crosstalk of acute lung and remote brain injury.

ACKNOWLEDGMENTS

We thank the staff of the animal research facility of the University of Würzburg, Germany, for their help in conducting the present study. Additionally, we are very grateful for the help of Verena Tretter from the Department of Anesthesia, General Intensive Care and Pain Management of the Medical University of Vienna, Austria, for analyzing proteomic and genomic samples. The excellent technical help of Magdeleine Herkt and Nicole Roder, Institute of Neuropathology of the University Medical Center of the Johannes Gutenberg-University Mainz, Germany, is kindly acknowledged.

REFERENCES

1. Ranieri VM, Rubenfeld GD, Thompson BT, et al; ARDS Definition Task Force: Acute respiratory distress syndrome: The Berlin Definition. *JAMA* 2012; 307:2526–2533
2. Quílez ME, López-Aguilar J, Blanch L: Organ crosstalk during acute lung injury, acute respiratory distress syndrome, and mechanical ventilation. *Curr Opin Crit Care* 2012; 18:23–28
3. Baumgardner JE, Otto CM, Markstaller K: Cyclic recruitment of atelectasis – Are there implications for our clinical practice? *Trends Anaesth Crit Care* 2014; 3:205–210
4. Williams EM, Viale JP, Hamilton RM, et al: Within-breath arterial PO_2 oscillations in an experimental model of acute respiratory distress syndrome. *Br J Anaesth* 2000; 85:456–459
5. Baumgardner JE, Markstaller K, Pfeiffer B, et al: Effects of respiratory rate, plateau pressure, and positive end-expiratory pressure on PaO_2 oscillations after saline lavage. *Am J Respir Crit Care Med* 2002; 166:1556–1562
6. Klein KU, Boehme S, Hartmann EK, et al: Transmission of arterial oxygen partial pressure oscillations to the cerebral microcirculation in a porcine model of acute lung injury caused by cyclic recruitment and derecruitment. *Br J Anaesth* 2013; 110:266–273
7. Klein KU, Hartmann EK, Boehme S, et al: PaO2 oscillations caused by cyclic alveolar recruitment can be monitored in pig buccal mucosa microcirculation. *Acta Anaesthesiol Scand* 2013; 57:320–325
8. Hartmann EK, Boehme S, Bentley A, et al: Influence of respiratory rate and end-expiratory pressure variation on cyclic alveolar recruitment in an experimental lung injury model. *Crit Care* 2012; 16:R8
9. Klein KU, Glaser M, Reisch R, et al: The effects of arterial carbon dioxide partial pressure and sevoflurane on capillary venous cerebral blood flow and oxygen saturation during craniotomy. *Anesth Analg* 2009; 109:199–204
10. Klein KU, Fukui K, Schramm P, et al: Human cerebral microcirculation and oxygen saturation during propofol-induced reduction of bispectral index. *Br J Anaesth* 2011; 107:735–741
11. Klein KU, Stadie A, Fukui K, et al: Measurement of cortical microcirculation during intracranial aneurysm surgery by combined laser-Doppler flowmetry and photospectrometry. *Neurosurgery* 2011; 69:391–398

12. Williams RW, Rakic P: Three-dimensional counting: An accurate and direct method to estimate numbers of cells in sectioned material. *J Comp Neurol* 1988; 278:344–352
13. Stummer W, Weber K, Tranmer B, et al: Reduced mortality and brain damage after locomotor activity in gerbil forebrain ischemia. *Stroke* 1994; 25:1862–1869
14. Frauenknecht K, Katzav A, Grimm C, et al: Neurological impairment in experimental antiphospholipid syndrome is associated with increased ligand binding to hippocampal and cortical serotonergic 5-HT1A receptors. *Immunobiology* 2013; 218:517–526
15. Diederich K, Quennet V, Bauer H, et al: Successful regeneration after experimental stroke by granulocyte-colony stimulating factor is not further enhanced by constraint-induced movement therapy either in concurrent or in sequential combination therapy. *Stroke* 2012; 43:185–192
16. Zilles K, Palomero-Gallagher N, Schleicher A: Transmitter receptors and functional anatomy of the cerebral cortex. *J Anat* 2004; 205:417–432
17. Zilles K, Wu J, Crusio WE, et al: Water maze and radial maze learning and the density of binding sites of glutamate, GABA, and serotonin receptors in the hippocampus of inbred mouse strains. *Hippocampus* 2000; 10:213–225
18. Hartmann EK, Ziebart A, Thomas R, et al: Inhalation therapy with the synthetic TIP-like peptide AP318 attenuates pulmonary inflammation in a porcine sepsis model. *BMC Pulm Med* 2015; 15:7
19. R Core Team (Eds): *R: A Language and Environment for Statistical Computing*. Vienna, Austria, R Foundation for Statistical Computing, 2012
20. Smyth GK: Limma: Linear models for microarray data. *In*: *Bioinformatics and Computional Biology Solutions Using R and Bioconductor*. Smyth GK (Ed). New York, Springer, 2005, pp 397–420
21. Sommer C, Fahrner A, Kiessling M: Postischemic neuroprotection in the ischemia-tolerant state gerbil hippocampus is associated with increased ligand binding to inhibitory GABA(A) receptors. *Acta Neuropathol* 2003; 105:197–202
22. Purves MJ: Fluctuations of arterial oxygen tension which have the same period as respiration. *Respir Physiol* 1966; 1:281–296
23. Folgering H, Smolders FD, Kreuzer F: Respiratory oscillations of the arterial PO_2 and their effects on the ventilatory controlling system in the cat. *Pflugers Arch* 1978; 375:1–7
24. Rocco PR, Dos Santos C, Pelosi P: Pathophysiology of ventilator-associated lung injury. *Curr Opin Anaesthesiol* 2012; 25:123–130
25. Bhatia M, Moochhala S: Role of inflammatory mediators in the pathophysiology of acute respiratory distress syndrome. *J Pathol* 2004; 202:145–156
26. Semenza GL: Oxygen sensing, homeostasis, and disease. *N Engl J Med* 2011; 365:537–547
27. Ward JP: Oxygen sensors in context. *Biochim Biophys Acta* 2008; 1777:1–14
28. Chen Q, Yu W, Shi J, et al: The effect of extracorporeal membrane oxygenation therapy on systemic oxidative stress injury in a porcine model. *Artif Organs* 2014; 38:426–431
29. Janz DR, Abel TW, Jackson JC, et al: Brain autopsy findings in intensive care unit patients previously suffering from delirium: A pilot study. *J Crit Care* 2010; 25:538.e7–538.12
30. Federico A, Cardaioli E, Da Pozzo P, et al: Mitochondria, oxidative stress and neurodegeneration. *J Neurol Sci* 2012; 322:254–262
31. Andrews ZB, Diano S, Horvath TL: Mitochondrial uncoupling proteins in the CNS: In support of function and survival. *Nat Rev Neurosci* 2005; 6:829–840
32. Dorszewska J: Cell biology of normal brain aging: Synaptic plasticity-cell death. *Aging Clin Exp Res* 2013; 25:25–34
33. Biegon A, Fry PA, Paden CM, et al: Dynamic changes in N-methyl-D-aspartate receptors after closed head injury in mice: Implications for treatment of neurological and cognitive deficits. *Proc Natl Acad Sci U S A* 2004; 101:5117–5122
34. Panerai RB: Cerebral autoregulation: From models to clinical applications. *Cardiovasc Eng* 2008; 8:42–59
35. Poulin MJ, Liang PJ, Robbins PA: Fast and slow components of cerebral blood flow response to step decreases in end-tidal PCO_2 in humans. *J Appl Physiol (1985)* 1998; 85:388–397
36. van Beek AH, Claassen JA, Rikkert MG, et al: Cerebral autoregulation: An overview of current concepts and methodology with special focus on the elderly. *J Cereb Blood Flow Metab* 2008; 28:1071–1085
37. Turalska M, Latka M, Czosnyka M, et al: Generation of very low frequency cerebral blood flow fluctuations in humans. *Acta Neurochir Suppl* 2008; 102:43–47
38. Zanatta P, Toffolo GM, Sartori E, et al: The human brain pacemaker: Synchronized infra-slow neurovascular coupling in patients undergoing non-pulsatile cardiopulmonary bypass. *Neuroimage* 2013; 72:10–19
39. Rivadulla C, de Labra C, Grieve KL, et al: Vasomotion and neurovascular coupling in the visual thalamus in vivo. *PLoS One* 2011; 6:e28746
40. Rayshubskiy A, Wojtasiewicz TJ, Mikell CB, et al: Direct, intraoperative observation of ~0.1 Hz hemodynamic oscillations in awake human cortex: Implications for fMRI. *Neuroimage* 2014; 87:323–331